Dean, Simon M., McNeill, Lisa C., Henstock, Timothy J., Bull, Jonathan M., Gulick, Sean P.S., Austin, James A., Bangs, Nathan L.B., Djajadihardja, Yusuf S. and Permana, Haryadi (2010). Contrasting Decollement and Prism Properties over the Sumatra 2004-2005 Earthquake Rupture Boundary. *Science*, 329, (5988), 207-210.(doi:10.1126/science.1189373).

Contrasting Decollement and Prism Properties over the Sumatra 2004-2005 Earthquake Rupture Boundary.

Simon M. Dean[1], Lisa C. McNeill[1], Timothy J. Henstock[1], Jonathan M. Bull[1], Sean P.S. Gulick[2], James A. Austin, Jr.[2], Nathan L.B. Bangs[2], Yusuf S. Djajadihardja[3], Haryadi Permana[4]

1 National Oceanography Centre, Southampton, University of Southampton, UK

2 Institute for Geophysics, Jackson School of Geosciences, University of Texas at Austin, USA

3 Agency for the Assessment and Application of Technology (BPPT), Indonesia

4 Research Center for Geotechnology, Indonesia Institute for Sciences, Indonesia

Styles of subduction zone deformation and earthquake rupture dynamics are strongly linked, impacting hazard potential. Seismic reflection profiles across the trench west of Sumatra show differences across the boundary between the major 2004 and 2005 plate interface earthquakes, which exhibited contrasting earthquake rupture and tsunami generation. In the southern part of the 2004 rupture, we interpret a negative polarity sedimentary reflector ~500m above the subducting oceanic basement as the seaward extension of the plate interface. This pre-décollement reflector corresponds to unusual prism structure, morphology and seismogenic behaviour in the southern 2004 rupture zone, characteristics absent along the 2005 rupture zone. Although the 2004 rupture zone is globally rare, our results show sediment properties influence earthquake rupture, tsunami hazard and prism development at subducting plate boundaries.

The Mw=9.2 Sumatra earthquake of 26 December 2004, initiated close to Simeulue Island, ruptured an area ~1300x150km and generated a regionally destructive tsunami (*1*). The Mw=8.7 28 March 2005 earthquake, immediately to the south across an apparently persistent rupture boundary, ruptured an area ~300x100km, causing only a local tsunami (*2*). Rupture offshore N. Sumatra in 2004 initiated at 30-40km depth, then propagated seaward beneath the prism and may have reached the seabed, rupturing faults within the prism (*3*; *4*; *5*). In contrast, the 2005 rupture largely occurred beneath the forearc basin and islands, with limited extent further seaward (*1*); other large subduction zone earthquakes such as Chile 1960 and Alaska 1964 similarly lack clear evidence for rupture close to the trench (e.g., *6*, *7*, *8*). These different rupture patterns are likely controlled by rheology (sediment properties), stress state and fault properties, and will generate different tsunami

by affecting both magnitude and water depth of the associated seafloor deformation. Sediment properties within the trench input section and forearc may also affect the morphology and deformation of the accretionary prism (e.g., *9*, *6*), in turn linked to the dynamic earthquake process (*10*). On some subduction margins (e.g., Nankai (*11*), Barbados (*12*)), a well-defined décollement (a low-angle detachment fault) into which accretionary prism faults sole, is identified as the plate boundary thrust. However, beneath the Sumatra forearc, the exact mechanism of rupture propagation and transfer of fault slip to the seafloor is poorly understood.

We collected 2500km of multichannel seismic reflection (MCS) profiles along the Sumatra margin from northwest of Simeulue Island to Nias Island (Fig. 1; *13*). Trench sediment velocities above oceanic basement are high (~4km/s) north of the 2004-5 rupture boundary, in contrast to equivalent sediments south of the rupture boundary (~3-3.5km/s; *13*, Fig. S1). North of the rupture boundary, a distinctive and regionally continuous high-amplitude negative polarity (HA-NP) reflector lies near the base of this trench deep ocean sediment section. We focus here on this reflector, which we believe represents the seaward extension of the plate boundary décollement, and thus is a key control on plate boundary and prism deformation along the Sumatran subduction zone.

The reflector is identified in MCS profiles perpendicular (Fig. 2) and parallel (Fig. 3) to the trench axis, typically ~0.5km above the top of the oceanic basement, within the ~4km/s high velocity layer (*13*), and has consistent character in all profiles. Its amplitude is higher than other sediment horizons more than 0.25km beneath the seabed, and is generally

stronger than the top oceanic basement reflector. The reflector's waveform is similar to the seabed and the seabed multiple (inset Fig. 2), and shows a clear negative polarity. The reflector may represent either a discrete layer, thinner than the seismic wavelength (<<100m) or a single interface between two units with contrasting seismic velocity and density. Mean reflection coefficients of at least -0.1 for the reflector versus 0.32 for the seabed (Table S1) indicate a major impedance decrease. We clearly image the reflector in the trench to the seaward end of our profiles from 2°N to 4°N (Fig. 1), up to ~35km from the deformation front. The reflector is less clearly imaged beneath the outer prism ~0.5km above the top of oceanic basement (Fig. 2), up to ~20km landward from the deformation front; the reflector has reduced amplitude and lateral continuity, possibly due to seismic imaging compromised by steep bathymetry and overlying prism fault structure, but retains negative polarity where observed.

The accretionary prism consists of fault-bounded blocks of relatively weakly deformed sediment. The vertical thickness of these blocks suggests that almost the entire incoming sediment section, to within ~500m of the top of the incoming plate, is accreted. We do not image the precise contact between the reflector and major outer-prism thrust faults, but these faults extend with ~45° dip from the seabed to at least 2km below the seafloor close to the reflector (Fig. 2), and we expect them to intersect the HA-NP reflector (inset Fig. 2).

Offshore of Simeulue, the trench seabed deepens by ~0.1km over ~50km towards the southeast, while the oceanic basement shallows by 1.75km (Fig. 3). The deep ocean

sediment layer thins and shallows over the rising basement with the basal ~0.75km of sediments (including the reflector) terminating against basement. Southeast of ~1°30'N, at the latitude of the 2005 rupture zone, the oceanic basement deepens again (e.g., Fig. 4) and subduction angle beneath the trench increases (*14*). The incoming sediment thickness is similar to the section just northwest of the basement high and stratigraphically we would expect the base of the sediments to be close to the depth of the HA-NP reflector observed to the northwest. However, no reflector with similar characteristics is observed and thus our data tightly constrain the southward limit of the HA-NP reflector. Stratigraphy of the deepest oceanic sediments seaward of Simeulue indicate that basement topography is pre-existing, probably related to an oceanic fracture zone (*14*).

The area where we observe the HA-NP reflector coincides with distinct accretionary prism properties and seismogenic behavior implying links to both long- and short-term deformation. The morphology and structure of the prism in this region are unusual: a steep outer slope and broad plateau extend up to 150km from the trench to the outer edge of the forearc basin (*3*). In contrast, the region to the southeast has a more uniform prism taper and reduced prism width of 100km (*15*). The southeastern termination of the reflector, close to the 2004-5 rupture boundary, also corresponds to a change in trend of the deformation front. The outer prism northwest of this change has well-developed landward-vergent fold ridges up to 80km long (*3*) compared with 20-30km long mixed-vergence folds to the southeast (*15*). Forearc islands are absent in the northwest even though free air gravity values are as high at the outer prism as in locations to the southeast. Finally, the aftershock distribution changes, consistent with the mainshock slip (*1*); aftershocks for the

2004 and 2005 events from the International Seismological Centre (ISC) catalogue (*16*; *13*) and from local networks (*17*) show epicenters extending to the trench where the reflector is present, while epicenters are rare in the seaward forearc where it is absent (Fig. 1). The aftershock distribution suggests that the reflector termination corresponds to the southern edge of 2004 seismicity within the outer prism.

High amplitude, negative polarity décollement and pre-décollement (the seaward extension of the décollement) reflectors are identified on several other convergent margins, most notably Northern Barbados (e.g., *12*; *18*; *19*; *20*), Nankai (e.g., *21*; *11*; *22*; *23*) and Central Cascadia (e.g., *24*). In N. Barbados, the décollement is locally HA-NP and traceable ~70-100km across the prism. Drilling and MCS data show reduced density, high porosity at the pre-décollement and décollement, resulting from high fluid content and underconsolidation and coincident with a weak radiolarian-rich claystone (*18; 19; 20*). In the Nankai Trough (Muroto transect), the pre-décollement is low amplitude and normal polarity, but the décollement is consistently HA-NP beneath the outer prism (*11)*. Drilling and MCS data show high pore fluid content reducing velocity and density and increasing porosity at and below the décollement, with fractures potentially enhancing porosity (*22*; *23*). Shallow décollements with high amplitude negative polarity reflections are weak faults (e.g., *18*; *19*) that can extend to depths of 10km beneath the prism and well into the seismogenic zone (*25*).

The reflector within the N. Sumatran trench sediments shares seismic characteristics with décollement horizons observed on other margins (e.g., N. Barbados, Nankai, C. Cascadia).

We infer that the horizon offshore N. Sumatra is a zone of low density and elevated pore pressure relative to overlying sediments. Such a layer, intrinsically weaker than surrounding sediments, would therefore be the likely locus for initiating the décollement fault, an interpretation consistent with the thickness of the frontally accreted sediment package. We infer that the landward extension of this horizon ultimately influences prism geometry and megathrust rupture. In N. Sumatra, the reflector has distinct properties up to 35km seaward of the deformation front, with a weaker negative polarity extension beneath the prism, rather than a strong negative reflector beneath the prism, and a weaker, variable polarity reflector seaward of the deformation front as observed on other margins. The reflector properties seaward of the deformation front imply a lithological origin on the N. Sumatra margin, rather than arising solely from structural or hydrogeological processes within the prism. Three changes could explain contrasting observed reflector properties southeast of the rupture boundary (Fig. 4): the stratigraphic section here post-dates the particular horizon; an equivalent stratigraphic section is present but has different lithologies; or the horizon properties differ due to combined differences in lithology and forearc deformational and hydrogeological processes across the rupture boundary. The deepest sediments in the northwest likely derive from the early Nicobar Fan (*26*) and the observed contrast in properties may be a result of oceanic basement highs limiting southward fan turbidite transport.

Multiple lines of evidence support interpretation of the distinct reflector as the pre-décollement/décollement on the N. Sumatran margin and we thus hypothesize that its landward extension acts as the focus of plate boundary slip as the seismogenic décollement.

Given the coincident changes in structure, seismic velocity, and seismogenic behaviour, the lithological and rheological properties of the lowermost sediments shown by the pre-décollement likely differ either side of the 2004-5 rupture boundary (Fig. 1) (*2*). Similarities between the structure and dynamics of the 2005 rupture segment and many other forearcs (e.g., *7*) emphasize the atypical nature of the southern 2004 rupture segment. Thus sediment properties may have a significant impact on earthquake rupture and tsunamigenesis by influencing décollement behavior from the trench deep into the seismogenic zone.

References and Notes

1. T. Lay *et al.*, *Science* **308**, 1127-1133 (2005).
2. R. W. Briggs *et al.*, *Science* **311,** 1897-1901 (2006).
3. T. J. Henstock, L. C. McNeill, D. R. Tappin, *Geology* **34**, 485-488 (2006).
4. E. Araki *et al.*, *Earth Planets Space* **58**, 113-119 (2006).
5. J.-C. Sibuet *et al.*, *Earth Plan. Sci. Lett.* **263**, 88-103 (2007).
6. D.E. Byrne, D.M. Davis, L.R. Sykes, *Tectonics,* **7**, 833-857 (1988).
7. R.E. Wells, R.J. Blakeley, Y. Sugiyama, D.W. Scholl, P.A. Dinterman, *J. Geophys. Res.*, **108**, B10, 2507 (2003).
8. G. Plafker, *J. Geophys. Res.* **77**, 901-925 (1972).
9. D. Davis, J. Suppe, F. A. Dahlen, *J. Geophys. Res.* **88**, 1153-1172 (1983).
10. K. L. Wang, Y. Hu, *J. Geophys. Res.* **111**, B06410 (2006).
11. N. L. Bangs *et al.*, *Geology* **32**, 273-276 (2004).
12. T. H. Shipley, G. F. Moore, N. L. Bangs, J. C. Moore, P. L. Stoffa, *Geology* **22**, 411-414 (1994).
13. Materials and methods are available as supporting material on *Science* Online.
14. D. Franke *et al., Earth Planet. Sci. Lett.* **269**, 118-130 (2008).
15. H. Kopp *et al., Basin Res.* **20**, 519-529 (2008).

16. International Seismological Centre, On-line Bulletin, http://www.isc.ac.uk (Internatl. Seis. Cent., Thatcham, United Kingdom, 2001).
17. F. Tilmann *et al.*, *Geophys. J. Int.*, doi :10.1111/j.1365-246X.2010.04597.x (2010).
18. N. L. Bangs, T. H. Shipley, J. C. Moore, G. F. Moore, *J. Geophys. Res.* **104**, 20399-20414 (1999).
19. J. C. Moore *et al.*, *Geology* **26**, 811-814 (1998).
20. J. C. Moore *et al.*, *Proc. Ocean. Drill. Program Sci. Results* **171A** (2000).
21. G. F. Moore, T. H. Shipley, *Proc. Ocean. Drill. Program Sci. Results* **131**, 73-82 (1993).
22. H. Mikada *et al.*, *Proc. Ocean. Drill. Program Init. Repts.* **196** (2002).
23. G. F. Moore, H. Mikada, J. C. Moore, K. Becker, A. Taira, *Proc. Ocean. Drill. Program Sci. Results* **190/196**, 1-26 (2005).
24. G. R. Cochrane, J. C. Moore, M. E. MacKay, G. F. Moore, *J. Geophys. Res.* **99**, 7033-7043 (1994).
25. N. L. Bangs *et al.*, *Earth Plan. Sci. Lett.* **284**, 44-49 (2009).
26. J. R. Curray, F. J. Emmel, D. G. Moore, *Mar. Petrol. Geol.* **19**, 1191-1223 (2003).
27. D. T. Sandwell, W. H. F. Smith, *J. Geophys. Res.* **114**, B01411 (2009).
28. C. Vigny, *et al.*, *Nature* **436**, 201-206 (2005).
29. D. Graindorge *et al.*, *Earth Planet. Sci. Lett.* **275**, 201-210 (2008).
30. We thank the Master and crew of the F/S Sonne and all those involved in SO198-2 for their assistance and our partners BPPT, Jakarta for their logistical assistance. This work was funded by NERC (NE/D004381/1) and NSF (OCE-0623165).

Figure Legends

Fig. 1. Multichannel seismic profiles (grey lines) and study area. Blue circles: December 2004 (solid) and March 2005 (open) Sumatra ISC earthquakes (*16*) one month post earthquake. Heavy black lines indicate seismic reflector observations; red lines locate Fig. 2

198 (A-A'), Fig. 3 (B-B') and Fig. 4 (C-C'). Dashed blue line: change in aftershock distribution
199 and southeastern boundary of distinct reflector. Green contours: 2004-5 coseismic uplift
200 (cm) on Simeulue Island (*2*); thin black lines: 1000m bathymetry contours; dotted black
201 contours indicate oceanic fracture zone from satellite-derived gravity data (*27*);
202 convergence vector from (*28*). Inset: multibeam bathymetry data (*3*; *14*; *29*).
203
204 Fig. 2. Depth-migrated seismic profile A-A' (distance from deformation front: DF). The
205 reflector continues from 7.25km depth in the southwest as a continuous negative polarity
206 event 0.2-0.5km above oceanic basement and discontinuously beneath outer prism (open
207 arrows). Red arrows: unconformity between trench fill and underlying deep ocean
208 sediment. Boxes show reflected waveforms: (A) seabed; (B) reflector (negative polarity);
209 top of oceanic basement near trace base (positive polarity); waveforms aligned at peak
210 amplitude. Inset shows schematic of prism structure and relationship to pre-décollement
211 (PD), décollement and seismogenic zone (SZ) northwest of 04-05 rupture boundary;
212 seismic sections shown represent outermost prism and oceanic plate.
213
214 Fig. 3. Depth-migrated trench-parallel seismic profile B-B' seaward of deformation front.
215 High-amplitude negative polarity reflector at 9.2km depth and oceanic basement ~10km in
216 northwest. Oceanic basement shallows by ~1.5km to southeast and reflector merges at 80-
217 85km along profile (black arrow). Red arrows indicate unconformity from Fig. 2. Inset
218 shows enlarged section of reflector (black box).
219
220 Fig. 4. Depth-migrated seismic profile C-C' plotted (distance from deformation front: DF).

Note higher amplitude oceanic basement reflector and thinner overlying oceanic sediment than in Fig. 1. Red arrows indicate unconformity from Fig. 2. A reflector, ~0.5km above oceanic basement, is superficially similar to the reflector identified in Figs. 2 and 3 but has significantly lower amplitude and variable polarity. Boxes A-D locate reflected waveforms shown in Fig. S6. Inset shows schematic of prism structure southeast of 04-05 rupture boundary.

Supporting Online Material

www.sciencemag.org

Materials and Methods

Figs. S1-S6

Table S1

Fig. 1

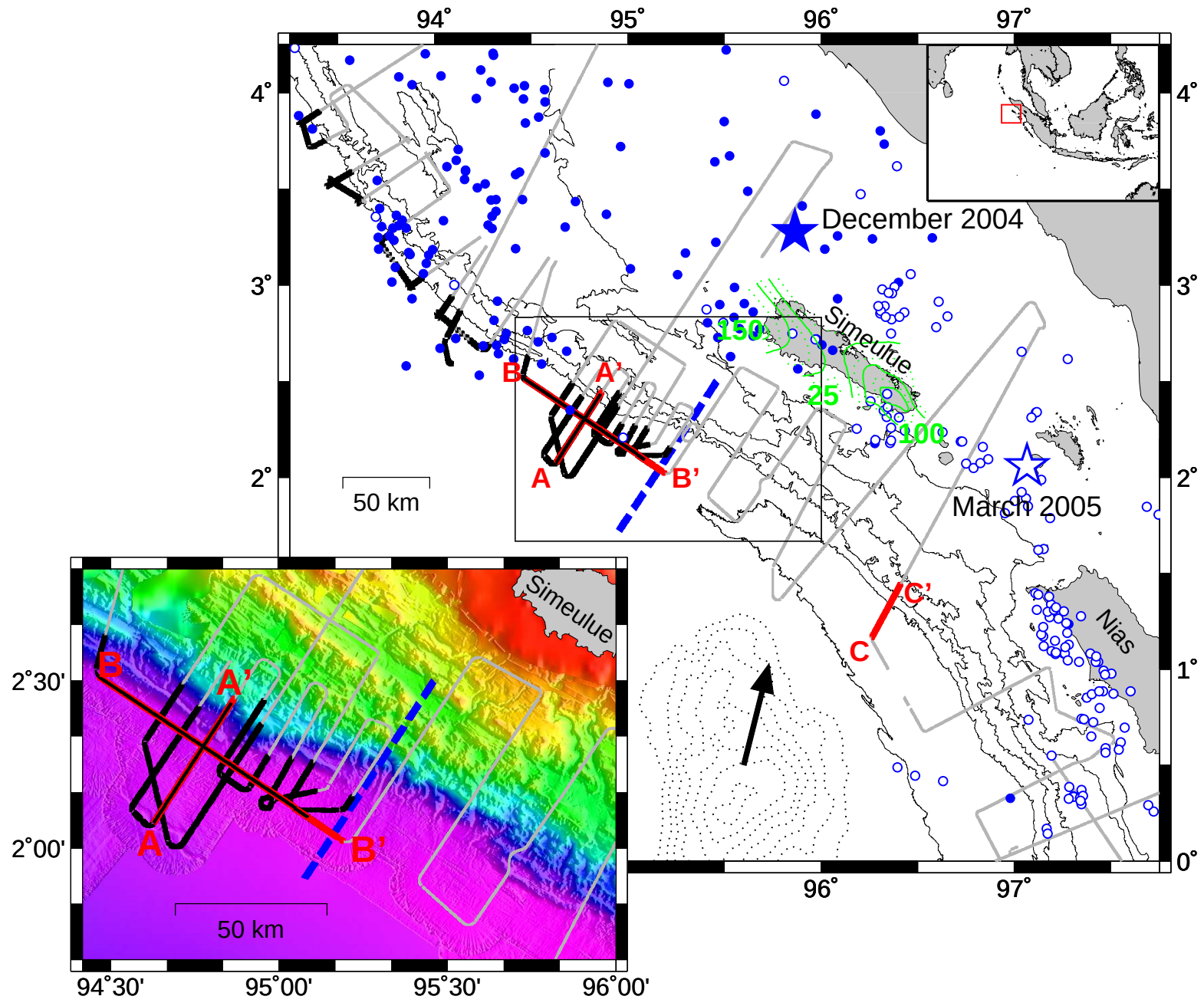
94°
95°
96°
97°
4°
3°
2°
1°
0°
December 2004
March 2005
Simeulue
Nias
150
25
100
A
A'
B
B'
C
C'
50 km
2°30'
2°00'
94°30'
95°00'
95°30'
96°00'

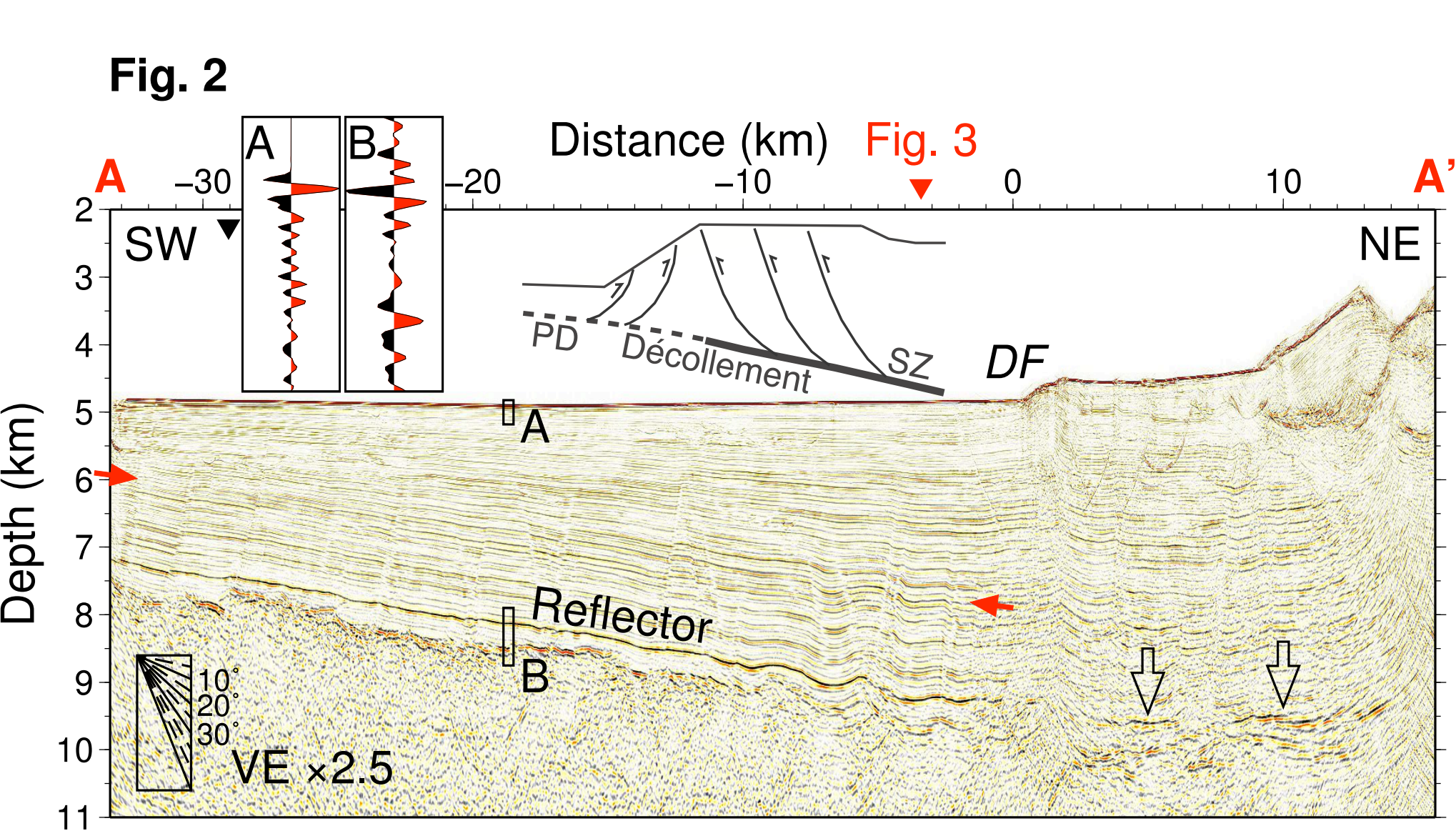
Fig. 2
A
B
Distance (km)
Fig. 3
A
A'
−30
−20
−10
0
10
SW
NE
PD
Décollement
SZ
DF
A
B
Reflector
10°
20°
30°
VE ×2.5
Depth (km)
2
3
4
5
6
7
8
9
10
11

Fig. 3

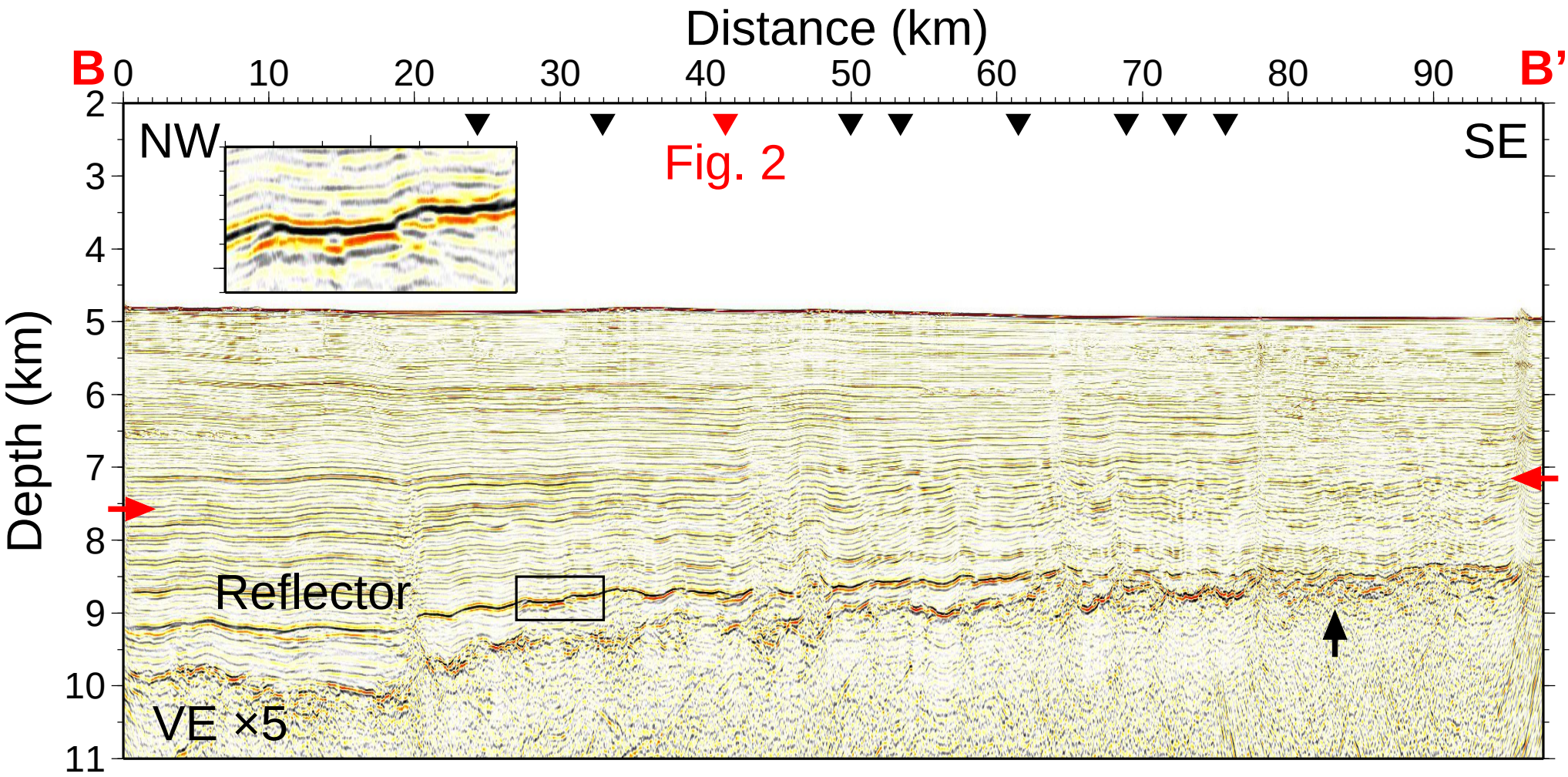
Distance (km)
B
B’
0
10
20
30
40
50
60
70
80
90
NW
SE
Fig. 2
Depth (km)
2
3
4
5
6
7
8
9
10
11
Reflector
VE ×5

Fig. 4

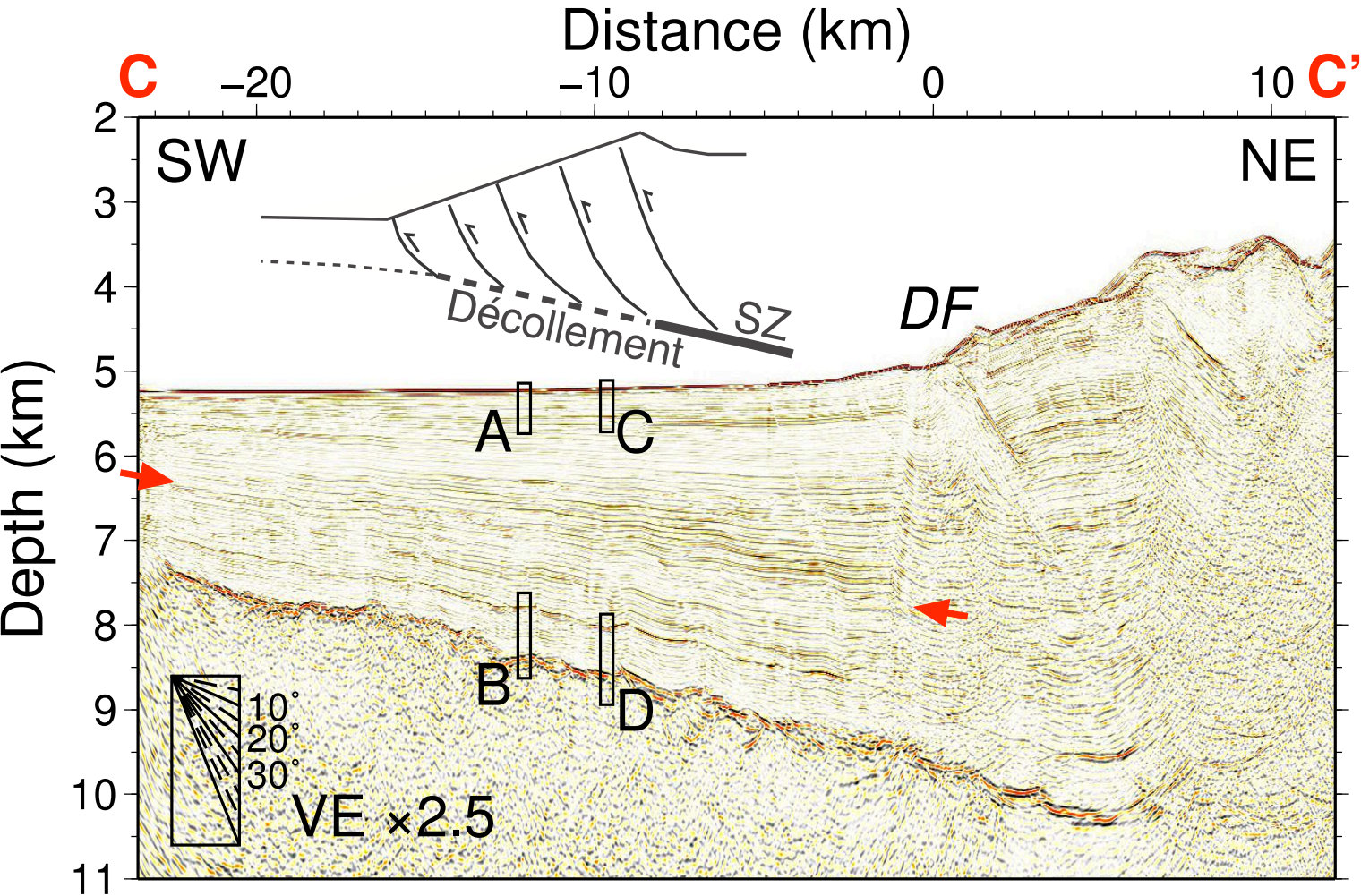
Distance (km)
C
C'
–20
–10
0
10
SW
NE
Décollement
SZ
DF
A
B
C
D
10°
20°
30°
VE ×2.5
Depth (km)
2
3
4
5
6
7
8
9
10
11